

Carbon Monoxide Oxidation by Atmospheric Oxygen on Catalysts Prepared by Pyrolysis of Transition Metal β -Diketonates on the Synthetic Foam Ceramics

I. I. Didenkulova^a, E. I. Tsyganova^a, V. M. Shekunova^a, and Yu. A. Aleksandrov^b

^a *Research Institute of Chemistry, Lobachevskii Nizhny Novgorod National Research University, pr. Gagarina 23, bld. 5, Nizhny Novgorod, 603950 Russia
e-mail: didenkul@mail.ru*

^b *Lobachevskii Nizhny Novgorod National Research University, Nizhny Novgorod, Russia*

Received October 18, 2010

Abstract—The results of development of new catalytic systems for the carbon monoxide oxidation to dioxide are systematized. The catalysts were produced by gas-phase thermal decomposition of the transition metal acetylacetonates on the synthetic foam ceramics. The kinetic and activation parameters of the oxidation on the catalysts were studied and their relative activity was explored. The activity of catalysts at the oxidation with air oxygen were found to depend on the nature of the deposited metal and the carrier. A synergistic effect in the bimetallic copper catalysts was revealed.

DOI: 10.1134/S1070363212010185

Carbon monoxide (CO) is a permanent component of the Earth's atmosphere, its natural content is 0.01–0.09 mg m⁻³. By the total mass, CO is the leader among the polluting emissions [1].

There are different approaches to the purification of gases: adsorption of polluting gas by a solid, absorption by a liquid, thermal decomposition, and the chemical catalytic methods. Among these, the chemical catalytic oxidation is the most promising, its application allows converting harmful impurities in the harmless or less harmful, and even in the useful substances [2].

Among the catalysts for CO oxidation not based on a noble metal, the intermetallides Al₃M (M = Gd, Y) [3], CdTe [4], high-temperature superconducting materials (HTSM) [5, 6] and metal oxides of the perovskite [7] and spinel [8, 9] structure have been investigated in sufficient detail. Among the supported catalysts not inferior in activity to the intermetallides and metal oxides a copper–cerium oxide catalysts containing 5 wt % Cu [10–13] should be noted; the high activity of the catalyst is due to the synergistic effect caused by the Cu–Ce interaction. Manufacturing of such supported catalysts is easier and consumes significantly less amount of active ingredients.

Undoubted effectiveness in CO oxidation showed the catalysts containing noble metals. Therewith, some catalysts are more active than pure metals [14] due to the presence of a “size effect” of positive nature: the reaction rate increases with the decrease in the size of the supported metal particles. This phenomenon greatly reduces the cost of some catalysts containing noble metals. However, at the use of such metals for catalyst preparation the problem of recycling raises and the use of additional processes and equipment to extract the active ingredient. Therefore, the use of the noble metals in catalytic systems leads to increase in expenses and thus limits their application to solving environmental problems.

Grainy, granular, and fibrous materials [9], and cellular metallic carriers with a high mechanical strength are used as catalysts [15]. A promising support for catalysts is the porous ceramics, which is advantageous due to the ability to form blocks.

It has been noted that the activity of catalytic systems is affected not only by the sequence of depositing oxides on the support [13], but also by the method of the catalyst preparation. Currently an intensive research of new methods of catalyst preparation is performed.

Table 1. The composition and properties of the ceramic carrier

| Comp. no. | Basic filler | Density ρ , g cm ⁻³ | Moisture capacity for 10 days, % | Specific surface area S_{sp} , m ² g ⁻¹ | Mechanical compressive strength, kg cm ⁻² | Porosity, % | Average pore size, r_{av} , nm |
|-----------|---------------------------|-------------------------------------|----------------------------------|---|--|-------------|----------------------------------|
| I | Natural clay ^a | 0.51 | 3.5 | 60.0 | 30.0 | 76 | 51 |
| II | Slurry GAZ ^b | 0.65 | 2.5 | 41.4 | 10.8 | 67 | 50 |

^a Clay of montmorillonite type. ^b Galvanic production wastes of Nizhny Novgorod automobile plant, containing, %: Cr³⁺ 0.017; Fe²⁺, Fe³⁺ 4.5; Mn²⁺ 0.01; Zn²⁺ 4.5; PO₄³⁻ 22.37; P₂O₅ 16.72; Cu²⁺ 0.01; Ni²⁺ 0.87; SO₄²⁻ 0.9; Cl⁻ 0.9.

In this study are systematized the results of the development of new catalytic systems for the oxidation of carbon monoxide on the basis of synthetic porous ceramics, which is durable, heat-resistant, and has a highly developed surface, being of low cost and containing a low concentration of active ingredient per unit of the surface area.

We studied the catalytic activity of the systems obtained by thermal decomposition of β -diketonates in a vacuum on a synthetic foam ceramics in the oxidation of carbon monoxide to dioxide [16–23]. We investigated the relative activity of various transition metals deposited on the ceramic media.

The carriers for the catalysts were prepared using a modified foam ceramics from HIPEK [24]. Table 1 lists the ceramic carrier composition and characteristics. The designed carriers and catalysts have medium density, an extended specific surface, high strength, high porosity, and low moisture content at saturation [22].

Thermograms of the obtained carriers annealed at 600°C for 2 h showed that the mass loss of the carrier **I** in the whole temperature range (35–900°C) did not exceed 0.25%. For the carrier **II** a melting above 760°C was noted, which limits the use of this carrier for the preparation of high-temperature catalysts. Thermograms of freshly prepared samples of carriers **I** and **II** showed that the process of structure formation of ceramic carrier is completed at 600°C [22].

The phase composition of the carriers was revealed by means of X-ray analysis of the annealed carrier **I**. Figure 1 shows the diffraction pattern of a sample as well as the theoretical diffraction patterns for a series of solid solutions.

The diffraction pattern of annealed ceramic sample **I** includes a set of peaks indicating a high degree of crystallinity of the obtained carrier [25]. The main reflections of ceramic carrier **I** correspond to the

trigonal-rhombohedral lattice of SiO₂ (α -quartz) and hexagonal lattice of SiO₂ of tridymite structure, and to aluminosilicate, mullite, iron oxide, and aluminum phosphate lattices. The data obtained are in good agreement with the composition of the ceramic carrier **I**, since for its synthesis natural clay was used containing in its composition the crystalline phases of aluminosilicate, quartz, tridymite and mullite; the crystalline phase of AlPO₄ has formed in the ceramic **I** during its synthesis.

The diffraction pattern of the carrier **II** because of the complexity of its chemical composition includes a large set of peaks indicating a mixture of crystalline substances [22].

The IR spectra of samples of ceramics **I** and **II** pressed, pre-crushed with KBr, were recorded on a Prestige 21 IR spectrometer. The spectra contain a strong broad band and several low-intensity bands in the frequency range 450 to 800 cm⁻¹, which can be attributed to the vibrations of silicate and sulfate groups in the composition of the carrier **I**. In the spectrum of carrier **II** these bands belong only to the vibrations of sulfate groups, since the silicon in its structure is absent [26, 27], but the two bands at 400–700 cm⁻¹ (572.38 cm⁻¹ and 668.34 cm⁻¹) are typical of complex oxides with perovskite structure [28]. The high-frequency band (668.34 cm⁻¹) is usually attributed to the M–O vibrations of a metal in octahedral coordination. The low-frequency band belongs to the vibrations of the M^I–O–M^{II} valence bonds. Deposition of metals on supports **I** and **II** did not change the type of infrared spectra, which is a consequence of low content (less than 5%) of the metal.

On the obtained carriers solid-phase products of thermal decomposition of transition metal acetylacetonates (M = Cu, Co, Mn, Zr, Fe, Cr), and nickel hexafluoroacetylacetonate Ni(hfacac)₂ were applied. In order to ensure uniform distribution of active ingredient, the gas-phase thermal decomposition of these

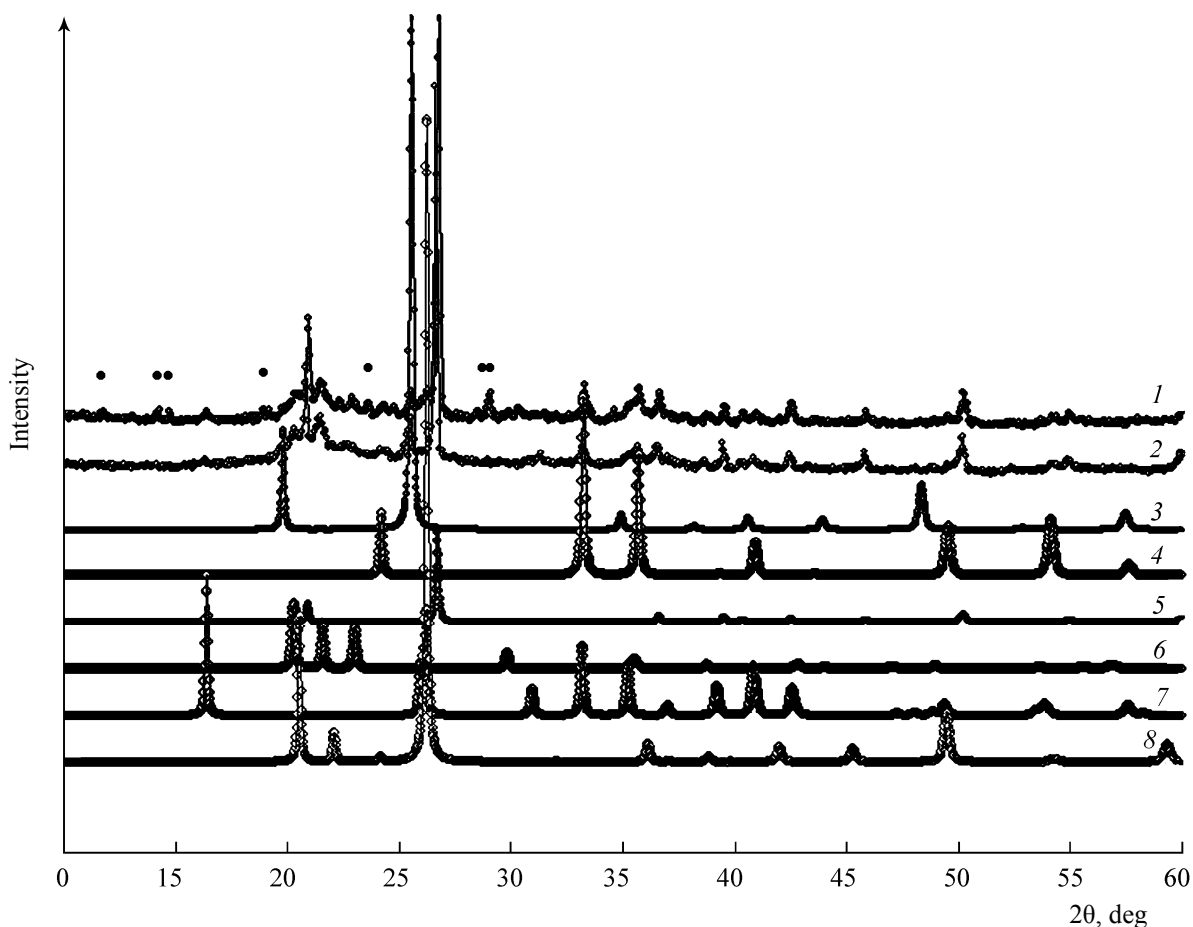


Fig. 1. Diffractogram of the catalysts Co–Cu/I on the ceramic carrier I (1) and the ceramic carrier I itself (2). Theoretical diffraction patterns according to the ICSD database: (3) aluminosilicate $\text{NaAlSi}_2\text{O}_6$, (4) Fe_2O_3 , (5) SiO_2 (α -quartz), (6) SiO_2 (tridymite), (7) $\text{Al}_{2.35}\text{Si}_{0.64}\text{O}_{4.82}$ (mullite), and (8) AlPO_4 . The non-identified peaks are marked by circles.

complexes in a vacuum (CVD) was carried out. Notation of the catalysts, the conditions of their preparation and processing are given in Table 2.

It is known that the thermal decomposition of metal β -diketonates gives composite coatings containing the metal, the respective oxide, carbide, and free carbon. All coatings were heated for 1 h at 600°C for the transformation of the metal in its oxide form and for the removal the unbound carbon.

The catalytic activity of different catalysts was compared by testing them in a pulse microcatalytic system. To compare the conversion approximately equal contact time: 0.7–0.8 s was used. Each catalyst was preliminarily heated in a reactor for 3 h at 500°C in a stream of helium to achieve a steady-state catalytic activity. The stationary state was reached by each catalyst after passing 2–3 times through the catalyst system the CO–air working mixture.

To calculate the kinetic parameters of the oxidation of CO to CO_2 in the pulse catalytic system we used the following equation [29]:

$$\ln \ln [1/(1-\alpha)] = -E_a^{\text{apparent}}/(RT) + \ln k_0.$$

The calculation of kinetic parameters with this equation is possible if the following conditions are fulfilled: the absence of chromatographic separation of reactants on the catalyst, the first total reaction order of the investigated reaction, the absence of the effects of diffusion factors on the process. These conditions have been maintained in this study.

We discovered and then set the conditions and parameters of the oxidation reaction in the pulse microcatalytic installation: the carrier gas flow rate 0.5 ml s^{-1} , the catalysts dispersion 0.3–0.5 mm, the CO and O_2 concentrations in the reaction mixture 2.6 and 20.0 vol %, respectively, the contact time for each catalyst 0.7–0.8 s.

Table 2. Composition of the catalysts for CO oxidation to CO₂ produced by CVD method, the conditions of their preparation and processing

| Catalyst composition | Notation | Metal source | Deposition conditions |
|----------------------------|----------|--|-----------------------|
| Carrier I + 3% Co | Co/I | Co(acac) ₂ | 320°C, 2 h |
| Carrier I + 3% Mn | Mn/I | Mn(acac) ₂ | 400°C, 1 h |
| Carrier I + 3% Zr | Zr/I | Zr(acac) ₄ | 350°C, 2 h |
| Carrier I + 3% Fe | Fe/I | Fe(acac) ₃ | 400°C, 1 h |
| Carrier I + 3% Cr | Cr/I | Cr(acac) ₃ | 400°C, 1 h |
| Carrier I + 3% Ni | Ni/I | Ni(hfacac) ₂ | 350°C, 1 h |
| Carrier I + 3% Cu | Cu/I | Cu(acac) ₂ | 350°C, 1 h |
| Carrier I + 3% Mn + 3% Ni | Mn-Ni/I | Mn(acac) ₂ Ni(hfacac) ₂ | 400°C, 1 h |
| Carrier I + 3% Mn + 3% Cu | Mn-Cu/I | Mn(acac) ₂ Cu(acac) ₂ | 400°C, 1 h |
| Carrier I + 3% Cu + 3% Ni | Cu-Ni/I | Cu(acac) ₂ Ni(hfacac) ₂ | 350°C, 1 h |
| Carrier I + 3% Co + 3% Cu | Co-Cu/I | Co(acac) ₂ Cu(acac) ₂ | 300°C, 2 h |
| Carrier I + 3% Co + 3% Ni | Co-Ni/I | Co(acac) ₂ Ni(hfacac) ₂ | 320°C, 1 h |
| Carrier II + 3% Co | Co/II | Co(acac) ₂ | 320°C, 2 h |
| Carrier II + 3% Mn | Mn/II | Mn(acac) ₂ | 400°C, 1 h |
| Carrier II + 3% Zr | Zr/II | Zr(acac) ₄ | 350°C, 2 h |
| Carrier II + 3% Fe | Fe/II | Fe(acac) ₃ | 400°C, 1 h |
| Carrier II + 3% Cr | Cr/II | Cr(acac) ₃ | 430°C, 1 h |
| Carrier II + 3% Ni | Ni/II | Ni(hfacac) ₂ | 350°C, 1 h |
| Carrier II + 3% Cu | Cu/II | Cu(acac) ₂ | 300°C, 1 h |
| Carrier II + 3% Mn + 3%Ni | Mn-Ni/II | Mn(acac) ₂ Ni(hfacac) ₂ | 400°C, 1 h |
| Carrier II + 3% Mn + 3%Cu | Mn-Cu/II | Mn(acac) ₂ Cu(acac) ₂ | 400°C, 1 h |
| Carrier II + 3% Cu + 3% Ni | Cu-Ni/II | Cu(acac) ₂ Ni(hfacac) ₂ | 350°C, 1 h |
| Carrier II + 3% Co + 3% Ni | Co-Ni/II | Co(acac) ₂ Ni(hfacac) ₂ | 300°C, 1 h |

The kinetic experiments conditions and the activation parameters of the heterogeneous catalytic oxidation of CO with air oxygen on the catalysts prepared by the CVD method on the carrier **I** are shown in Table 3. Calculation of the apparent activation energy was performed using the data up to 50% conversion in the region of the absence of side reactions and the kinetic mode of the process, as evidence the values of activation energies obtained.

The carrier **I** was characterized by a weak catalytic activity in CO oxidation: the beginning of conversion occurred at 450°C, and the 50% conversion was observed at 810°C (Fig. 2). The carrier **II** showed a complicated form of the dependence of conversion on temperature. The conversion begins at 220°C in the temperature range 300–700°C, the conversion ranges from 40 to 47% and then raises sharply with increasing temperature.

Table 3. Activation parameters of catalytic oxidation of CO to CO₂ on the catalysts prepared by CVD method in the presence of oxygen, on the ascending branch of hysteresis

| Catalysis | ΔH_{298}^0 (M–O), kJ mol ⁻¹ | Hysteresis mode | Temperature range, °C | T , °C for α 50% | log k_0 | E_a^{apparent} , kJ mol ⁻¹ |
|------------|---|------------------|--------------------------|------------------------------|-----------|---|
| Co-Cu/I | | – | 100–250 | 215 | 4.4±1.1 | 42.2±2.7 |
| Cu-Ni/I | | Counterclockwise | 97–300 | 215 | 4.9±0.3 | 47.9±2.8 |
| Cu/I | 266.7 | – | 170–370 | 275 | 4.3±0.7 | 48.1±6.7 |
| Ni/I | 364.1 | Clockwise | 170–473 | 300 | 4.4±0.5 | 49.8±2.2 |
| Co-Ni/I | | – | 150–700 | 300 | 3.6±0.2 | 41.2±5.2 |
| Mn-Cu/I | | Clockwise | 140–450 | 335 | 3.7±0.1 | 44.3±1.1 |
| Cr/I | 456.0 | – | 210–590 | 380 | 2.9±0.2 | 35.4±2.8 |
| Co/I | 368.3 | Counterclockwise | 255–408 | 400 | 9.5±1.2 | 121.0±3.7 |
| Mn/I | 409.6 | Counterclockwise | 300–690 | 540 | 4.3±0.1 | 68.3±1.8 |
| Zr/I | 757.4 | Counterclockwise | 300–630 | 575 | 7.1±1.6 | 97.8±4.1 |
| Fe/I | 410.1 | – | 300–685 | 600 | 3.1±0.1 | 55.6±3.3 |
| Mn-Ni/I | | – | 200–780 | 670 | 3.2±0.1 | 60.5±2.1 |
| Carrier I | | – | 450–840 | 810 | 2.1±0.2 | 47.8±2.9 |
| Co-Ni/II | | – | 200–350 | 240 | 6.6±0.1 | 69.1±2.4 |
| Cu/II | 266.7 | – | 185–632 | 260 | 5.8±0.2 | 61.7±3.4 |
| Ni/II | 364.1 | – | 240–392 | 290 | 8.0±1.2 | 89.4±2.8 |
| Co/II | 368.3 | Counterclockwise | 170–370 | 323 | 12.0±1.1 | 137.9±2.8 |
| Fe/II | 410.1 | – | 200–394 | 345 | 9.8±0.7 | 112.7±3.5 |
| Cr/II | 456.0 | Counterclockwise | 275–740 | 400 | 4.7±0.3 | 62.5±3.6 |
| Zr/II | 757.4 | Counterclockwise | 250–780 | 470 | 6.0±1.2 | 82.2±4.5 |
| Mn-Ni/II | | Clockwise | 300–700 | 615 | 2.7±0.2 | 48.1±2.4 |
| Mn-Cu/II | | Clockwise | 327–700 | 620 | 2.5±0.1 | 44.8±1.1 |
| Mn/II | 409.6 | Clockwise | 450–750 | 725 | 1.7±0.5 | 40.6±4.0 |
| Cu-Ni/II | | – | 600–800 | 765 | 6.0±0.3 | 121.9±4.9 |
| Carrier II | | – | 220–800 | 500 | 9.1±1.2 | 101.9±3.9 |

This phenomenon may be due to a change in the oxidation state of the transition metal in the carrier composition, and the presence on the carrier surface of perovskite-like structures (detected by IR spectroscopy) that are active catalysts for CO oxidation. However, the perovskite surface bears not only the oxidation sites, but also the sites of side reactions, the latter in the temperature range 300–600°C can strongly

bind up to 95% of CO, thus limiting the conversion raise in this temperature range [28].

Application of composite coatings on carriers significantly increased their catalytic activity. We compared the catalytic activity of catalysts in the presence of oxygen at the a temperature corresponding to 50% conversion on the ascending branch of the hysteresis loop.

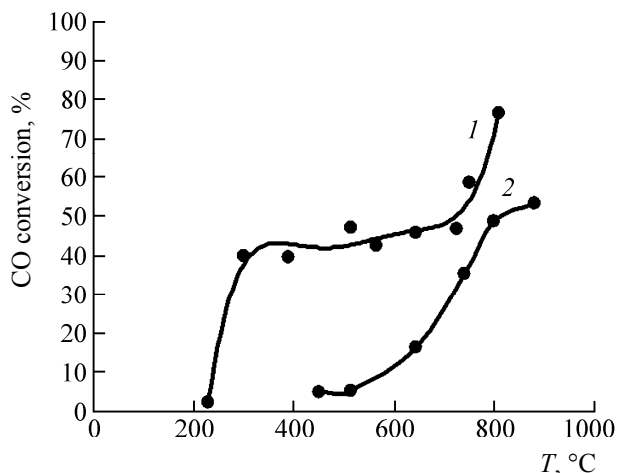


Fig. 2. Comparison of catalytic activity of the carriers **I** and **II** ($F = 0.5 \text{ cm}^3 \text{ s}^{-1}$, the fraction 0.3–0.5 mm). (1) carrier **II**, (2) carrier **I**.

The data in Table 3 indicate that the studied catalysts on the carrier **I** can be arranged in the following series by their catalytic activity: $\text{Co-Cu} \geq \text{Cu-Ni} > \text{Cu} > \text{Ni} \geq \text{Co-Ni} > \text{Mn-Cu} > \text{Cr} > \text{Co} > \text{Mn} > \text{Zr} > \text{Fe} > \text{Mn-Ni}$. The most active catalysts on the carrier **I** were those promoted with the metal-containing solid products of the thermal decomposition of the Co–Cu or Cu–Ni β -diketonate mixtures. On these catalysts the reaction started already at 100°C and complete conversion of CO to CO₂ was observed at 250–300°C. Figures 3 and 4 show the typical conversion curves for the catalysts on the carrier **I**.

As seen from Fig. 3, the activity of monometallic catalysts Cu/**I** and Ni/**I** is lower than that of the bimetallic catalyst Cu–Ni/**I**. The same effect is observed in the case of monometallic catalysts Co/**I**, Cu/**I** (Fig. 4) and bimetallic Co–Cu/**I**.

The high activity of copper–nickel and copper–cobalt catalysts (Figs. 3 and 4) in the oxidation of CO is due to a synergistic effect caused by the interaction of ions Cu–Co and Cu–Ni, where, as in the case of copper–cerium catalysts [10], copper can be easily integrated into the lattice of cobalt and nickel oxides. The replacement by the Cu⁺ leads to the appearance of oxygen vacancies that causes high mobility of oxygen in the catalyst lattice resulting in the high activity of the binary copper catalysts.

The least active in the oxidation of carbon monoxide was Mn–Ni/**I** catalyst. Moreover, its activity was much lower than that of the monometallic catalysts Ni/**I** and Mn/**I**. In this case an antagonism

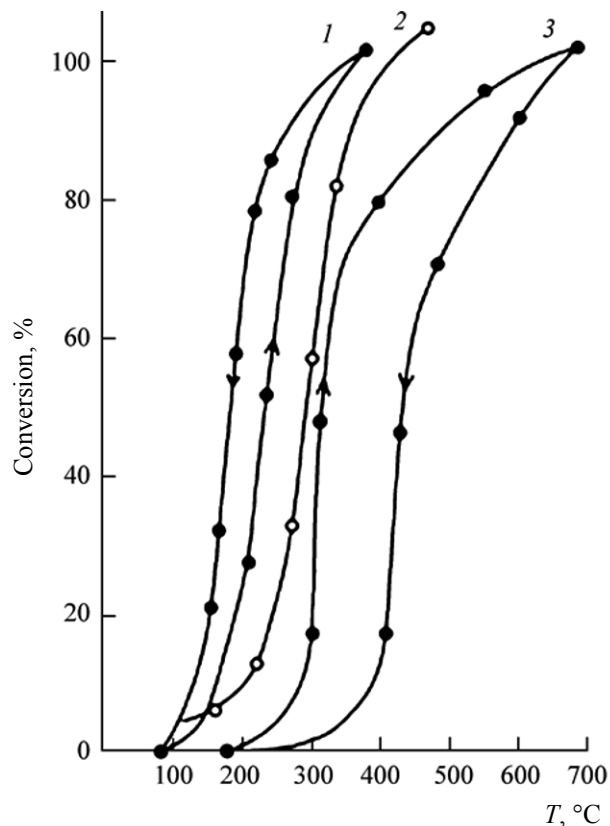


Fig. 3. Comparison of catalytic activity of catalysts on the carrier **I** ($F = 0.5 \text{ cm}^3 \text{ s}^{-1}$, the fraction 0.3–0.5 mm). Catalysts: (1) Cu–Ni/**I**, (2) Cu/**I**, (3) Ni/**I**.

occurs in coupling the ions affecting the catalytic activity on the catalyst surface. It is known [30] that octahedrally coordinated metal ions on the surface of complex oxide catalyst play a special role, determining mainly the catalytic activity. The decrease in the activity of binary catalysts containing manganese oxides is a result of relatively easy oxidation of the Mn²⁺ to Mn³⁺ and Mn⁴⁺, which have octahedral coordination and displace more active ions (in this case Ni) from the octahedral sites to the tetrahedral.

It was previously found [31] that the rate of catalytic oxidation of CO to CO₂ varies with changes in the size of deposited particles of the active component, that is, the CO oxidation is structure-sensitive. In the case of Mn-containing catalysts (Mn/**I**) the “size effect” of the negative nature was observed (the reaction rate decreased with the decrease in the size of the particles deposited on the carrier). In the case of Co-, Cr- and Ni-containing catalysts the “size effect” is positive in nature (the reaction rate increases). In the case of Fe-containing catalysts, we are dealing with structure-insensitive reaction.

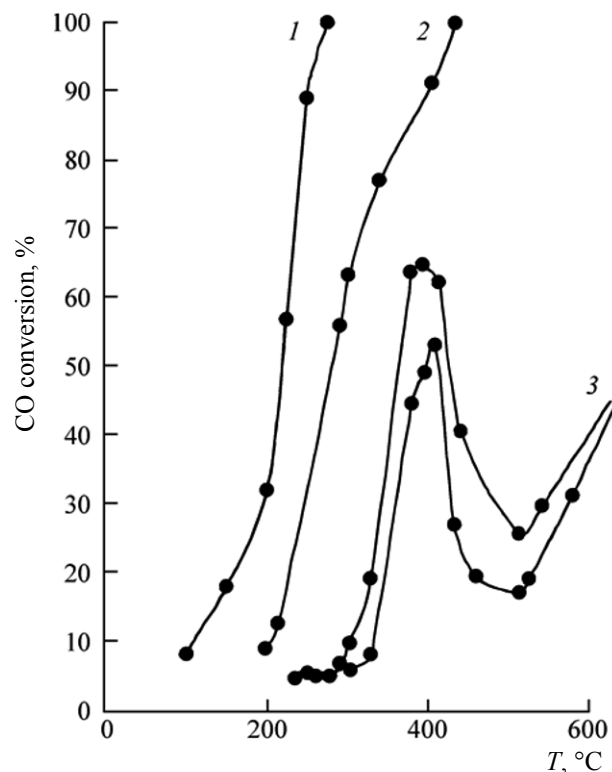


Fig. 4. Comparison of catalytic activity of the oxidation catalysts on carrier I ($F = 0.5 \text{ cm}^3 \text{ s}^{-1}$, the fraction 0.3–0.5 mm). Catalysts: (1) Co–Cu/I, (2) Cu/I, (3) Co/I.

The studied monometallic catalysts based on the carrier I form the following series by their catalytic activity in CO oxidation with atmospheric oxygen (at the temperature of 50% conversion, along the ascending branch of the hysteresis loop): Cu > Ni > Cr > Co > Mn > Zr > Fe.

This series is in accordance with the values of the metal–oxygen bond energy (Table 3): the lower is the M–O bond energy, the more active is the catalyst.

The study showed that the most active on the carrier I are the bimetallic catalysts, especially copper-containing, except for the Mn–Ni catalyst. The catalysts prepared on the basis of carrier I operate stably over a wide temperature range up to 1000°C.

The study of the catalysts on the carrier II gave the following series of activities: Co–Ni > Cu > Ni > Co > Fe > Cr > Zr > Mn–Ni \geq Mn–Cu > Mn > Cu–Ni.

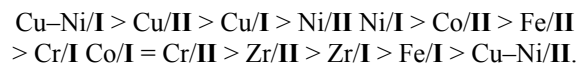
The reaction on the most active Co–Ni catalyst begins at 200°C, and the complete conversion of CO to CO₂ was observed at 350°C. The least active was the Cu–Ni catalyst. It should be noted that in contrast to the catalysts based on the carrier I, on the carrier II the monometallic catalysts are more active than the

bimetallic ones. The monometallic catalysts based on the carrier II give the following series by their catalytic activity in CO oxidation with atmospheric oxygen: Cu > Ni > Co > Fe > Cr > Zr > Mn. This series of catalysts is in good agreement with the values of the energy of the metal–oxygen bond.

It should be noted that the plots of conversion of CO to CO₂ on the catalysts based on carrier II have complex undulate form, with maxima and minima in the kinetic curves (Figs. 5 and 6). This nature of the conversion is due to the complex composition of the carrier II that consists mainly of salts (chlorides, sulfates, and phosphates) of transition metals and contains the perovskite-like structures on its surface.

The curves of the conversion–temperature dependence of some catalysts supported on I and II reflect the phenomenon of “hysteresis,” when the values of conversion is not the same at the raise and decrease in the temperature (Figs. 3, 5). The hysteresis is observed both “counterclockwise,” e.g., Co/I, Mn/I, Cu–Ni/I, Zr/I (carrier I) and Co/II, Cr/II, Zr/II (carrier II), and, commonly seldom, “clockwise,” Ni/I and Mn–Cu/I (carrier I), and Mn/II, Mn–Cu/II and Mn–Ni/II (carrier II). The occurrence of hysteresis can be due to different factors: the presence of critical phenomena and the multiplicity of stationary states, the change in the phase composition of the catalyst and the different forms of adsorbed oxygen, as well as by local overheating of active centers and low thermal conductivity of porous media.

The activity in the presence of oxygen of all the studied catalysts, with the exception of the Mn-containing ones, forms the following series (at the temperature of 50% conversion):



This sequence indicates that monometallic catalysts of oxidation on the support II are more active than those on the support I. Also a great difference is seen in the activity of Cu–Ni catalysts supported on I or II ($\Delta T = 550^\circ\text{C}$ at 50% conversion), which may be associated with the presence of poisoning the catalyst by chloride ions in the carrier II. This series is also in good agreement with the energy of the M–O bond.

Thus, by the study of catalytic systems for CO oxidation obtained by CVD method on the carriers I and II it was found that the activity of the catalysts depends not only on the activity of the metal on the

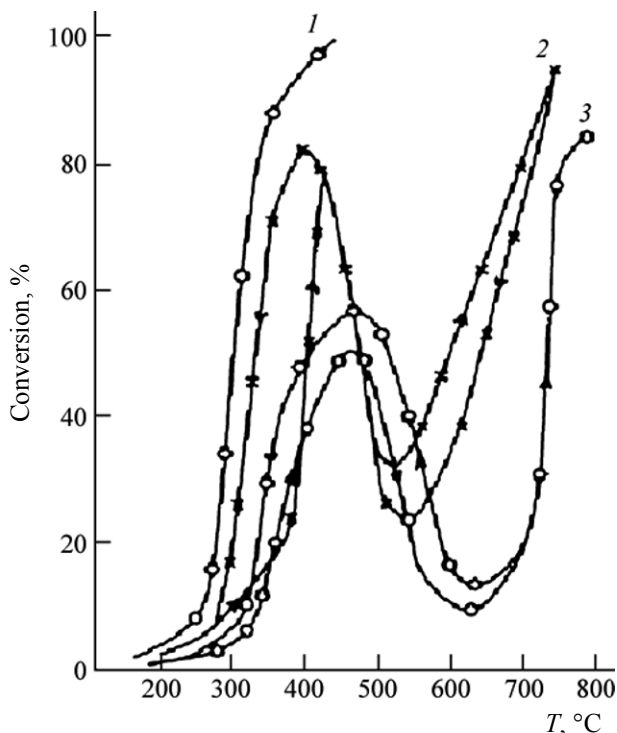


Fig. 5. Comparison of catalytic activity of catalyst on the carrier **II** ($F = 0.5 \text{ cm}^3 \text{ s}^{-1}$, the fraction 0.3–0.5 mm). Catalysts: (1) Fe/**II**, (2) Cr/**II**, (3) Zr/**II**.

carrier surface, but also on the nature of the carrier itself. Supported catalyst on **I** are more versatile, because they retain the activity in a wide range of temperatures, while the carrier **II** melts at the temperature above 760°C .

Previously [16, 17] by the example of Cu- and Co-containing catalysts prepared on a carrier **II** we have shown that the mode of the metal deposition affects the catalyst. The greatest catalytic activity up to 50% conversion had the catalyst prepared by pyrolysis of $\text{Cu}(\text{acac})_2$ along the CVD method. The catalyst prepared by impregnating the carrier with the $(\text{CH}_3\text{COO})_2\text{Cu}$ solution is close to it by the activity. This is due to the similarity of the solid phase compositions formed at the decomposition of copper acetate and acetylacetonate. The lowest activity had Cu/**II** catalyst prepared with the introduction of copper nitrate in the carrier composition at the preparation of the latter. Its activity was the same as the activity of the carrier **II** itself. This is explained by location of CuO inside the carrier bulk and in its internal pores,

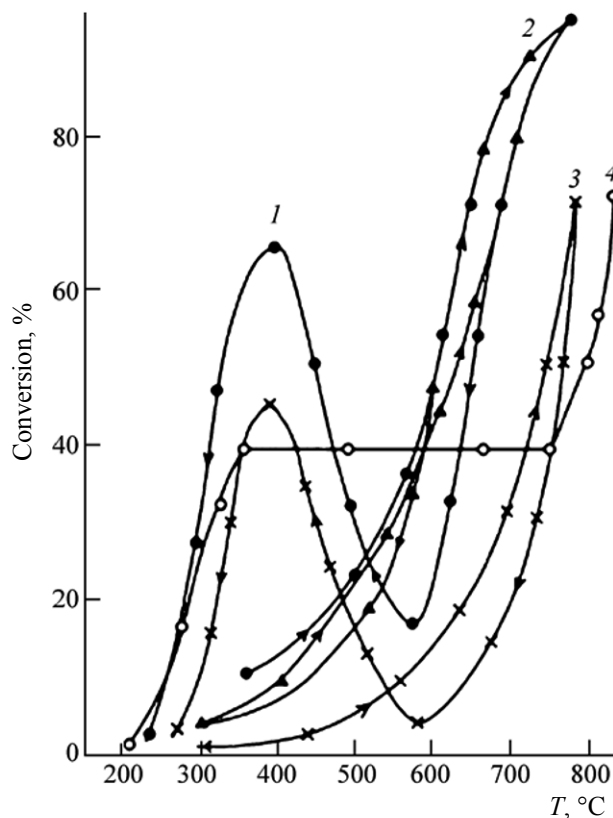


Fig. 6. Comparison of catalytic activity of Mn-containing catalysts for CO oxidation on a carrier **II** ($F = 0.5 \text{ cm}^3 \text{ s}^{-1}$, the fraction 0.3–0.5 mm). Catalysts: (1) Mn-Ni/**II**, (2) Mn-Cu/**II**, (3) Mn/**II**, (4) carrier **II** itself.

while in the heterogeneous catalysis the oxidation of CO proceeds on the outer surface of the catalyst. A similar pattern was observed for the Co-containing catalysts. The best was Co-containing catalyst on a carrier **II**, produced by CVD method: on this catalyst the conversion began at 170°C , and 80% conversion probability was achieved at 340°C .

Thus, the catalysts prepared by deposition in a vacuum from the gas phase (CVD) are superior by their catalytic properties to catalysts prepared by conventional impregnation. The catalysts on an inert carrier **I** (the base is natural clay of the montmorillonite type) are heat resistant up to 1000°C . The most active are the catalysts promoted with metal-containing solid product of thermal decomposition of a mixture of Co-Cu or Cu-Ni β -diketonates.

EXPERIMENTAL

Preparation of carriers for catalysts based on a "HIPEK" ceramics was performed in accordance with

TU 5759-010-10657190-97 [24], by introducing various fillers and additives to the system. To prepare the catalyst were taken the ceramic samples annealed for 1 h at 500°C (fraction of 0.3–0.5 mm).

The carrier-promoting additive ratios are given in Table 2. A weighed sample of the carrier with pre-calculated amount of a β -diketonate was placed in a 60 ml glass ampule, the ampule was evacuated and placed in a furnace heated to a desired temperature. The optimum conditions for thermal decomposition of β -diketonates were chosen [32]. The obtained catalysts were annealed at 600°C in air for 1 h.

Kinetics of heterogeneous catalytic oxidation of CO to CO₂ was studied using a pulsed version of gas chromatographic method. Conversion was calculated from the intensity of CO₂ peaks using the method of calibration. The technique of kinetic measurements is described in [33].

The IR spectra of pressed samples pre-crushed with KBr of the carriers **I** and **II** and catalysts based on them were recorded on a Shimadzu infrared Fourier spectrometer IR Prestige 21.

The X-ray diffraction (XRD) studies were performed on a DRON-3M diffractometer using CuK α radiation with a graphite monochromator on the diffracted beam. Registration was carried out in the angular range $2\theta = 10^\circ$ – 60° with 0.05° steps of 2θ at 2 s exposure per point.

Thermogravimetric (TGA) analysis was performed on a Perkin-Elmer PYRIS 6 TGA unit. The 24 mg samples were placed in platinum crucibles. The linear polythermal heating option was used for the analysis with the rate of 5°C min^{-1} in air. The air flow rate was 80 ml min^{-1} . The maximum heating temperature was 900°C . The sensitivity of the instrument is $1\text{ }\mu\text{g}$, the accuracy 0.2%.

REFERENCES

1. *Vrednye khimicheskie veshchestva* (Harmful Chemical Substances), Filov, V.A., Ed., Leningrad: Khimiya, 1988.
2. Tiunov, L.A. and Kustov, V.V., *Toksikologiya okisi ugleroda* (Carbon Monoxide Toxicology), Moscow: Meditsina, 1980.
3. Kononenko, V.I., Chupova, I.A., Shevchenko, V.G., and Torokin, V.V., RF Patent no. 2279911, 2004, *Byul. Izobret.*, 2006, no. 20.
4. Kirovskaya, I.A., Fedyaeva, O.A., and Mironova, E.I., RF Patent no. 2308321, 2006, *Byul. Izobret.*, 2007, no. 29.
5. Berentsveig, V.V., Lagutkina, O.I., and Shabatin, V.P., *Kinetika i Kataliz*, 1992, vol. 33, nos. 5–6, p. 1174.
6. Bobolev, A.V., Borisov, Yu.V., and Vydrin, S.N., *Fizikokhimiya i tekhnologiya vysokotemperaturnykh sverkhprovodyashchikh materialov* (Physical Chemistry and Technology of High-Temperature Superconducting Materials), Moscow: Nauka, 1989.
7. Panich, N.M., Pirogova, G.N., Korosteleva, R.I., and Voronin, Yu.V., *Izv. Akad. Nauk, Ser. Khim.*, 1999, no. 4, p. 698.
8. Pirogova, G.N., Panich, N.M., Korosteleva, R.I., Voronin, Yu.V., and Popova, P.N., *Izv. Akad. Nauk, Ser. Khim.*, 2000, no. 9, p. 1547.
9. Eyubova, S.M. and Yagodovskii, V.D., *Zh. Fiz. Khim.*, 2007, vol. 81, no. 4, p. 637.
10. Il'ichev, A.N., Firsova, A.A., and Korchak, V.N., *Kinetika i Kataliz*, 2006, vol. 47, no. 4, p. 602.
11. Snytnikov, P.V., Stadnichenko, A.I., Semin, G.L., Belyaev, V.D., Boronin, L.I., and Sobyenin, V.A., *Kinetika i Kataliz*, 2007, vol. 48, no. 3, p. 472.
12. Snytnikov, P.V., Stadnichenko, A.I., Semin, G.L., Belyaev, V.D., Boronin, L.I., and Sobyenin, V.A., *Kinetika i Kataliz*, 2007, vol. 48, no. 3, p. 463.
13. Firsova, A.A., Il'ichev, A.N., Khomenko, T.N., Gorobinskii, L.V., Maksimov, Yu.V., Suzdalev, I.P., and Korchak, V.N., *Kinetika i Kataliz*, 2007, vol. 48, no. 2, p. 298.
14. Boudart, M., *Advances in Catalysis*, 1969, vol. 20, p. 153.
15. Semikolenov, V.A., *Zh. Prikl. Khim.*, 1997, vol. 70, no. 5, p. 785.
16. Tsyganova, E.I., Didenkulova, I.I., Shekunova, V.M., Faerman, V.I., and Aleksandrov, Yu.A., *Zh. Obshch. Khim.*, 2004, vol. 74, no. 11, p. 1770.
17. Tsyganova, E.I., Didenkulova, I.I., Shekunova, V.M., and Aleksandrov, Yu.A., *Zh. Obshch. Khim.*, 2004, vol. 74, no. 5, p. 742.
18. Tsyganova, E.I., Didenkulova, I.I., Shekunova, V.M., and Aleksandrov, Yu.A., *Zh. Obshch. Khim.*, 2005, vol. 75, no. 9, p. 1426.
19. Tsyganova, E.I., Didenkulova, I.I., Shekunova, V.M., and Aleksandrov, Yu.A., *Zh. Obshch. Khim.*, 2005, vol. 75, no. 10, p. 1678.
20. Tsyganova, E.I., Didenkulova, I.I., Shekunova, V.M., and Aleksandrov, Yu.A., *Vestn. Nizhegorod. Gos. Univ., Ser. Khim.*, 2007, no. 2, p. 95.
21. Didenkulova, I.I., Tsyganova, E.I., Shekunova, V.M., and Aleksandrov, Yu.A., *Vestn. Nizhegorod. Gos. Univ., Ser. Khim.*, 2007, no. 3, p. 257.
22. Didenkulova, I.I., Tsyganova, E.I., Shekunova, V.M., Kirillov, A.I., Pishchurova, I.A., and Aleksandrov, Yu.A., *Vestn. Nizhegorod. Gos. Univ., Ser. Khim.*, 2008, no. 3, p. 79.

23. Didenkulova, I.I., Tsyganova, E.I., Shekunova, V.M., and Aleksandrov, Yu.A., Abstract of Papers, *4th Ssesion of Scientific School of the Seminar "Industrial and Ecological Safety,"* Sarov: RFYaTs-VNIIEF, 2004, p. 15.
24. Aleksandrov, Yu.A., Tsyganova, E.I., Shekunova, V.M. and Didenkulova, I.I., RF Patent no. 2345973, 2008, *Byul. Izobret.*, 2009, no. 4.
25. Kovba, L.M. and Trunov, V.K., *Rentgenofazovyi analiz (X-Ray Analysis)*, Moscow: Mosk. Gos. Univ., 1976, p. 148.
26. Nakamoto, K., *Infrared and Raman Spectra of Inorganic and Coordination Chemistry*, Moscow: Mir, 1966, p. 151.
27. Bellamy, L., *The Infrared Spectra of Complex Organic Molecules*, Moscow: Inostrannaya Literatura, 1963.
28. Panich, N.M., Pirogova, G.N., Korosteleva, R.I., and Voronin, Yu.V., *Izv. Akad. Nauk, Ser. Khim.*, 1999, no. 4, p. 698.
29. Bassett, D.W. and Habgood, H.W., *J. Phys. Chem., A*, 1960, vol. 64, p. 769.
30. Jacobs, J.P., Maltha, L., Reintjes, J.G., Drimal, J., Ponec, V., and Brongersma, H.H., *J. Catal.*, 1994, vol. 147, p. 294.
31. Anufrienko, V.F., Moroz, B.L., Larina, T.V., Ruzan-kin, S.F., Bukhtiyarov, V.I., and Parmon, V.N., *Dokl. Akad. Nauk*, 2007, vol. 313, no. 4, p. 493.
32. Suvorova, O.N., Varyukhin, V.A., and Kutyreva, V.V., *Primenenie metalloorganicheskikh soedinenii dlya polucheniya neorganicheskikh pokrytii i materialov (Application of Organometallic Compounds for Obtaining Coverings and Materials)*, Razuvaev, G.A., Ed., Moscow: Nauka, 1986, p. 68.
33. Aleksandrov, Yu.A., Tsyganova, E.I., Ivanovskaya, K.E., and Vorozheikin, I.A., *Zh. Obshch. Khim.*, 2002, vol. 72, no. 1, p. 17.